CRYSTAL GROWTH & DESIGN

ARTICLE

pubs.acs.org/crystal

Three Transition-Metal Substituted Polyoxotungstates Containing Keggin Fragments: From Trimer to One-Dimensional Chain to Two-Dimensional Sheet

Lijuan Chen, Dongying Shi, Junwei Zhao,* Yulong Wang, Pengtao Ma, Jingping Wang, and Jingyang Niu*

Institute of Molecular and Crystal Engineering, College of Chemistry and Chemical Engineering, Henan University, Kaifeng, Henan 475004, P. R. China

Supporting Information

ABSTRACT: Three novel transition-metal substituted polyoxotungstates based on Keggin fragments, $Cs_3K_3[Co(H_2O)_6]_2[Co(H_2O)_3(\alpha\text{-}GeW_{11}CoO_{38})_3]\cdot 30H_2O$ (**1**), $K_{18}\{[Mn(H_2O)_3]_2[Mn(H_2O)_2][(B\text{-}\beta\text{-}SiW_9O_{33}(OH))Mn_3(H_2O)(B\text{-}\beta\text{-}SiW_8O_{30}(OH))]_2\}\cdot 16H_2O$ (**2**), and $K_8[Cd(H_2O)_3]_2[Cd_4(H_2O)_2(B\text{-}\alpha\text{-}SiW_9O_{34})_2]\cdot 20H_2O$ (**3**), have been synthesized by reaction of dilacunary Keggin precursors $K_8[\gamma\text{-}GeW_{10}O_{36}]\cdot 6H_2O$/$K_8[\gamma\text{-}SiW_{10}O_{36}]\cdot 12H_2O$ with transition-metal salts at ambient temperature and characterized by inductively coupled plasma (ICP) analyses, IR spectra, UV spectra, and single-crystal X-ray diffraction. The polyoxoanion of **1** is a novel trimer constructed from three mono-Co^{II} substituted Keggin fragments $[\alpha\text{-}GeW_{11}CoO_{38}]^{4-}$ linked by six W−O−Co/W bridges and a capping $[Co(H_2O)_3]^{2+}$ bridge. **2** displays the one-dimensional chain built by tetrameric $\{[Mn(H_2O)_3]_2[Mn(H_2O)_2][(B\text{-}\beta\text{-}SiW_9O_{33}(OH))Mn_3(H_2O)(B\text{-}\beta\text{-}SiW_8O_{30}(OH))]_2\}^{18-}$ units, which is the first one-dimensional silicotungstate containing asymmetric sandwich-type moieties constructed from $[B\text{-}\beta\text{-}SiW_9O_{34}]^{10-}$ and $[B\text{-}\beta\text{-}SiW_8O_{31}]^{10-}$ fragments. **3** utilizes the two-dimensional sheet established by tetra-Cd^{II} substituted sandwich-type $[Cd_4(H_2O)_2(B\text{-}\alpha\text{-}SiW_9O_{34})_2]^{12-}$ units and $[Cd(H_2O)_3]^{2+}$ linkers, representing the first two-dimensional (3,6)-topological network with a Schläfli symbol of $3^64^65^3$ built by sandwich-type Keggin units in polyoxometalate chemistry. Magnetic susceptibility measurements indicate antiferromagnetic exchange interactions within Co^{II} ions in **1** and within Mn^{II} ions in **2**. The best least-squares fitting values for **2** are $J = -1.16\ cm^{-1}$ and $g = 2.13$ based on the isotropic spin model. Furthermore, the room-temperature solid-state photoluminescence of **3** displays two emission bands, which are derived from O → Cd ligand-to-metal charge transfer transitions and O → W ligand-to-metal charge transfer transitions, respectively.

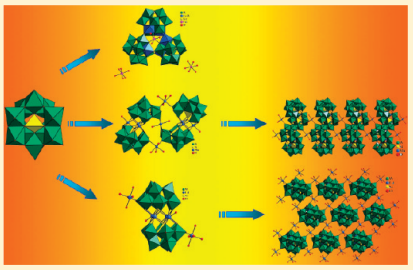

INTRODUCTION

Polyoxometalates (POMs) are a unique class of fascinating metal−oxygen cluster species of early transition metals with enormous structural varieties and interesting properties leading to actual and potential applications in catalysis, medicine, material science, and magnetism.[1] In the past several decades, increasing interest in POMs has been predominantly driven by the widespread applications, which has inspired the search for novel transition-metal substituted polyoxometalates (TMSPs) with unexpected structures and properties. Thus, lacunary POM precursors are usually used as inorganic nucleophilic polydentate ligands to incorporate transition-metal (TM) centers into the matrixes of POMs constructing giant TMSP aggregates and multidimensional frameworks.[2]

Within the family of lacunary POM precursors, dilacunary Keggin polyoxoanions mainly refer to $[\gamma\text{-}GeW_{10}O_{36}]^{8-}$ and $[\gamma\text{-}SiW_{10}O_{36}]^{8-}$, because both can be easily isolated in the form of potassium salts. The dilacunary decatungstogermanate $K_8[\gamma\text{-}GeW_{10}O_{36}]\cdot 6H_2O$ was first prepared by Kortz et al. in 2006.[3] Since then, its reactivities with organometal or various TM ions were exploited by Kortz'group.[4] In 2006, a novel benzene-Ru^{II}-supported dilacunary decatungstogermanate $[\{Ru(C_6H_6)(H_2O)\}\{Ru(C_6H_6)\}(\gamma\text{-}GeW_{10}O_{36})]^{4-}$ was reported.[4a] Later, several unusual TM substituted tungstogermanates $[K(H_2O)(\beta\text{-}Fe_2GeW_{10}O_{37}(OH))(\gamma\text{-}GeW_{10}O_{36})]^{12-}$,[4b] $[\{\beta\text{-}Fe_2GeW_{10}O_{37}(OH)_2\}_2]^{12-}$,[4b] $[Cu_3(H_2O)(B\text{-}\beta\text{-}GeW_9O_{33}(OH))(B\text{-}\beta\text{-}GeW_8O_{30}(OH))]^{12-}$,[2m] and $[M(H_2O)_2\{M_3(B\text{-}\beta\text{-}GeW_9O_{33}(OH))(B\text{-}\beta\text{-}GeW_8O_{30}(OH))\}_2]^{22-}$ (M = Co^{II}, Mn^{II})[2m] were isolated. In 2009, Cronin et al. communicated a Keggin-based trimeric aggregate $[Rb\subset(GeW_{10}Mn_2O_{38})_3]^{17-}$.[5] On the other hand, the dilacunary decatungstosilicate $K_8[\gamma\text{-}SiW_{10}O_{36}]\cdot 12H_2O$ was first synthesized by Teze et al.[6] To date, the research on its reaction with organometal or TM ions has been extensively performed.[7] For example, in 1996, Zhang et al. and Wassermann et al. reacted it with Mn^{II} and Cr^{III} cations, respectively, and obtained disubstituted products with the retained γ-framework.[7a,b] Meanwhile, Xin et al. synthesized a phenyltin substituted dimer $[(PhSnOH_2)_2(\gamma\text{-}SiW_{10}O_{36})_2]^{10-}$.[7c] In 1999−2004, Kortz et al. investigated the interactions of this polyanion with

Received: January 19, 2011
Revised: March 9, 2011
Published: March 22, 2011

Ni^{II}, Cu^{II}, Mn^{II}, Zn^{II}, and Ti^{IV} cations and isolated the dimeric $[\{\beta\text{-}SiNi_2W_{10}O_{36}(OH)_2(H_2O)\}_2]^{12-}$,[7d] sandwich-type $[\{SiM_2W_9O_{34}(H_2O)\}_2]^{12-}$ (M = Cu^{II}, Mn^{II}, Zn^{II}),[7e] cyclic trimeric $[(\beta_2\text{-}SiW_{11}MnO_{38}OH)_3]^{15-}$,[7f] and wheel tetrameric $[\{\beta\text{-}Ti_2SiW_{10}O_{39}\}_4]^{24-}$.[7g] In 2001, Mizuno et al. studied the catalytic performance of $[\gamma\text{-}SiW_{10}\{Fe^{III}(OH_2)\}_2O_{38}]^{6-}$ for the selective epoxidation of alkenes with molecular oxygen at 1 atm,[1b] and in 2003, they reported the good catalytic performance of $[\gamma\text{-}SiW_{10}O_{34}(H_2O)_2]^{4-}$ for the epoxidation of various olefins.[7h] In 2005−2006, Kortz and co-workers explored the reactions of $K_8[\gamma\text{-}SiW_{10}O_{36}]\cdot 12H_2O$ with Co^{II}, Zr^{IV}, and $[Ru(C_6H_6)Cl_2]_2$, leading to $[Co_6(H_2O)_{30}\{Co_9Cl_2(OH)_3(H_2O)_9(\beta\text{-}SiW_8O_{31})_3\}]^{5-}$,[7i] $[\{Co_3(B\text{-}\beta\text{-}SiW_9O_{33}(OH))(B\text{-}\beta\text{-}SiW_8O_{29}(OH)_2)\}_2]^{22-}$,[7j] $[Zr_6O_2(OH)_4(H_2O)_3(\beta\text{-}SiW_{10}O_{37})_3]^{14-}$,[7k] $[Zr_4O_2(OH)_2(H_2O)_4(\beta\text{-}SiW_{10}O_{37})_2]^{10-}$,[7k] and $[\{Ru(C_6H_6)(H_2O)\}\{Ru(C_6H_6)\}(\gamma\text{-}SiW_{10}O_{36})]^{4-}$.[4a] In 2006−2007, Hill et al. addressed several dilacunary multi-Fe^{III} substituted γ-Keggin silicotungstates $[\{Fe_2(OH)_3(H_2O)_2\}_3(\gamma\text{-}SiW_{10}O_{36})_3]^{15-}$,[7l] $[\{Fe(OH)(OAc)\}_4(\gamma\text{-}SiW_{10}O_{36})_2]^{12-}$,[7m] and $[\{Fe_6(OH)_9(H_2O)_2(OAc)_2\}(\gamma\text{-}SiW_{10}O_{36})_3]^{17-}$[7m] and evaluated the former catalytic aerobic oxidation activity.[7l] At the same time, several interesting TM substituted silicotungstate magnetic clusters $[\{(\gamma\text{-}SiW_{10}O_{36})Mn_2(OH)_2(N_3)_{0.5}(H_2O)_{0.5}\}_2(\mu\text{-}1,3\text{-}N_3)]^{10-}$,[7n] $[(\gamma\text{-}SiW_{10}O_{36})_2Cu_4(\mu\text{-}1,1,1\text{-}N_3)_2(\mu\text{-}1,1\text{-}N_3)_2]^{12-}$,[7n] $[\{(B\text{-}\beta\text{-}SiW_9O_{33}(OH))(\beta\text{-}SiW_8O_{29}(OH)_2)Co_3(H_2O)\}_2Co(H_2O)_2]^{20-}$,[7o] and $[Co_{1.5}(H_2O)_7][(\gamma\text{-}SiW_{10}O_{36})(\beta\text{-}SiW_8O_{30}(OH))Co_4(OH)(H_2O)_7]^{7-}$[7o] were prepared by Mialane et al. In 2007−2008, a 2-D sandwich-type silicotungstate $\{[Ni(dap)_2(H_2O)]_2[Ni(dap)_2]_2[Ni_4(Hdap)_2(\alpha\text{-}B\text{-}HSiW_9O_{34})_2]\}\cdot 7H_2O$ and a 1-D chain monocopper^{II}-substituted Keggin silicotungstate $\{[Cu(en)_2(H_2O)]_2[Cu(en)_2][\alpha\text{-}SiCuW_{11}O_{39}]\}\cdot 5H_2O$ were hydrothermally prepared by us by means of reacting $K_8[\gamma\text{-}SiW_{10}O_{36}]\cdot 12H_2O$ with $NiCl_2\cdot 6H_2O$ or $CuCl_2\cdot 2H_2O$ in the presence of 1,2-diaminopropane or ethylenediamine.[2j,7p] Recently, we launched the exploration on the reactions of dilacunary Keggin $[\gamma\text{-}XW_{10}O_{36}]^{8-}$ (X = Ge^{IV}, Si^{IV}) precursors with TM cations in the conventional aqueous solution at room temperature based on the following considerations: (a) The dilacunary Keggin $[\gamma\text{-}XW_{10}O_{36}]^{8-}$ precursors are often metastable and labile (certainly, they can also retain their original γ-framework if conditions are appropriate), can transform to plenary, monolacunary, trilacunary, and even tetralacunary Keggin POM units, and can also isomerize to the α- and β-framework, which provides the possibility for the structural variety of desired products. (b) In previously reported documents, the molar ratios of TM cations/dilacunary Keggin precursors are mostly lower than 5; however, the system with their molar ratios higher than 5 remains largely unexplored,[7i,k,2j,p] which offers us a good opportunity to exploit this domain with the aim of discovering novel TMSPs. (c) Using the principle of chemical equilibrium, increasing the amount of a reactant can make a reaction move toward the desired direction. Under the guidance of these considerations, three novel TMSPs based on lacunary Keggin fragments, $Cs_3K_3[Co(H_2O)_6]_2[Co(H_2O)_3(\alpha\text{-}GeW_{11}CoO_{38})_3]\cdot 30H_2O$ (**1**), $K_{18}\{[Mn(H_2O)_3]_2[Mn(H_2O)_2][(B\text{-}\beta\text{-}SiW_9O_{33}(OH))Mn_3(H_2O)(B\text{-}\beta\text{-}SiW_8O_{30}(OH))]_2\}\cdot 16H_2O$ (**2**), and $K_8[Cd(H_2O)_3]_2[Cd_4(H_2O)_2(B\text{-}\alpha\text{-}SiW_9O_{34})_2]\cdot 20H_2O$ (**3**), have been successfully obtained by controlling the higher molar ratios of TM cations/dilacunary Keggin precursors at room temperature and structurally characterized by ICP analyses, IR spectra, UV spectra, and single-crystal X-ray diffraction. The polyoxoanion skeleton of **1** is a novel trimeric oligomer constructed from three mono-Co^{II} substituted Keggin fragments $[\alpha\text{-}GeW_{11}CoO_{38}]^{4-}$ linked by six W−O−Co/W bridges and a capping $[Co(H_2O)_3]^{2+}$ bridge. **2** displays the one-dimensional chain built by rare tetrameric $\{[Mn(H_2O)_3]_2[Mn(H_2O)_2][(B\text{-}\beta\text{-}SiW_9O_{33}(OH))Mn_3(H_2O)(B\text{-}\beta\text{-}SiW_8O_{30}(OH))]_2\}^{18-}$ units, which is the first one-dimensional silicotungstate containing asymmetric sandwich-type moieties constructed from $[B\text{-}\beta\text{-}SiW_9O_{34}]^{10-}$ and $[B\text{-}\beta\text{-}SiW_8O_{31}]^{10-}$ fragments. **3** exhibits the two-dimensional sheet established by tetra-Cd^{II} substituted sandwich-type $[Cd_4(H_2O)_2(B\text{-}\alpha\text{-}SiW_9O_{34})_2]^{12-}$ units and $[Cd(H_2O)_3]^{2+}$ linkers, representing the first two-dimensional (3,6)-topological network with a Schläfli symbol of $3^64^65^3$ built by sandwich-type Keggin units in polyoxometalate chemistry. Magnetic susceptibility measurements indicate antiferromagnetic exchange interactions within Co^{II} ions in **1** and within Mn^{II} ions in **2**. The best least-squares fitting values for **2** are $J = -1.16\ cm^{-1}$ and $g = 2.13$ based on the isotropic spin model. Furthermore, the photoluminescence of **3** has been studied.

EXPERIMENTAL SECTION

General Methods and Materials. All chemicals were commercially purchased and used without further purification. $K_8[\gamma\text{-}GeW_{10}O_{36}]\cdot 6H_2O$ and $K_8[\gamma\text{-}SiW_{10}O_{36}]\cdot 12H_2O$ were synthesized according to the literature[3,6] and characterized by IR spectra. ICP analyses were performed on a Perkin-Elmer Optima 2000 ICP-OES spectrometer; IR spectra were obtained from a solid sample palletized with KBr on an Nicolet 170 SXFT-IR spectrometer in the range 400−4000 cm^{-1}. UV−vis spectra were obtained with a U-4100 spectrometer at room temperature. Magnetic measurements were carried out with a Quantum Design MPMS-XL-7 magnetometer in the temperature range 2−300 K. The susceptibility data were corrected from the diamagnetic contributions as deduced by using Pascal's constant tables. Emission/excitation spectra were recorded on a F-7000 fluorescence spectrophotometer.

Synthesis of $Cs_3K_3[Co(H_2O)_6]_2[Co(H_2O)_3(\alpha\text{-}GeW_{11}CoO_{38})_3]\cdot 30H_2O$ (1). $K_8[\gamma\text{-}GeW_{10}O_{36}]\cdot 6H_2O$ (1.473 g, 0.507 mmol) was dissolved in 10 mL of water at room temperature, and then $CoCl_2\cdot 6H_2O$ (2.377 g, 9.990 mmol) and CsCl (0.300, 1.782 mmol) were successively added with stirring. The resulting mixture was stirred for 1.5 h and filtered. The filtrate was left to slowly evaporate at room temperature. Red prismatic crystals of **1** appeared after several days. The product was isolated by filtration and then air-dried. Yield: *ca.* 40% (based on $K_8[\gamma\text{-}GeW_{10}O_{36}]\cdot 6H_2O$). Anal. Calcd (found %) for $H_{90}Co_6Cs_3Ge_3K_3O_{159}W_{33}$ (**1**): Co 3.61 (3.78), Cs 4.07 (3.98), K 1.20 (1.34), Ge 2.23 (2.13), W 61.98 (61.84). IR (KBr pellet): 3407(s), 1624(m), 951(s), 874(s), 783(s), 714(s), 515(m), 454(m) cm^{-1}.

Synthesis of $K_{18}\{[Mn(H_2O)_3]_2[Mn(H_2O)_2][(B\text{-}\beta\text{-}SiW_9O_{33}(OH))Mn_3(H_2O)(B\text{-}\beta\text{-}SiW_8O_{30}(OH))]_2\}\cdot 16H_2O$ (2). $K_8[\gamma\text{-}SiW_{10}O_{36}]\cdot 12H_2O$ (0.741 g, 0.249 mmol) was dissolved in 15 mL of 1 M HAc/NaAc buffer (pH 5.0), and then $MnCl_2\cdot 4H_2O$ was added (0.252 g, 1.273 mmol). The resulting mixture was stirred for 1.5 h and filtered. Slow evaporation at room temperature led to yellow prismatic crystals suitable for X-ray diffraction after several days. The product was isolated by filtration and then air-dried. Yield: *ca.* 36% (based on $K_8[\gamma\text{-}SiW_{10}O_{36}]\cdot 12H_2O$). Anal. Calcd (found %) for $H_{72}K_{18}Mn_9O_{156}Si_4W_{34}$ (**2**): M_n 4.88 (5.01), K 6.95 (6.89), Si 1.11 (1.20), W 61.71 (61.58). IR (KBr pellet): 3437(s), 1624(m), 944(s), 905(sh), 875(s), 722(s), 530(s) cm^{-1}.

Synthesis of $K_8[Cd(H_2O)_3]_2[Cd_4(H_2O)_2(B\text{-}\alpha\text{-}SiW_9O_{34})_2]\cdot 20H_2O$ (3). The synthetic procedure of **2** was employed with $3CdSO_4\cdot 8H_2O$ (0.660 g, 0.858 mmol) replacing $MnCl_2\cdot 4H_2O$. Colorless prismatic crystals were obtained after several days. Yield: *ca.* 42% (based on $K_8[\gamma\text{-}SiW_{10}O_{36}]\cdot 12H_2O$). Anal. Calcd (found %) for

Table 1. Crystallographic Data and Structural Refinements for 1−3

	1	2	3
formula	$H_{90}Co_6Cs_3Ge_3K_3O_{159}W_{33}$	$H_{72}K_{18}Mn_9O_{156}Si_4W_{34}$	$H_{56}Cd_6K_8O_{96}Si_2W_{18}$
M_r (g mol^{-1})	9789.15	10130.10	5945.13
T (K)	296(2)	296(2)	296(2)
crystal system	monoclinic	triclinic	monoclinic
space group	$P2_1/n$	$P\bar{1}$	C_2/c
a (Å)	13.371(3)	12.722(11)	23.838(8)
b (Å)	33.458(8)	17.742(16)	12.084(4)
c (Å)	36.582(9)	20.620(19)	30.450(10)
α (deg)	90	91.844(15)	90
β (deg)	95.539(4)	107.857(15)	96.985(5)
γ (deg)	90	108.924(15)	90
V (Å^3)	16290(7)	4145(6)	8706(5)
Z	4	1	4
D_c (g cm^{-3})	3.992	4.058	4.536
μ (mm^{-1})	25.177	24.722	25.639
limiting indices	$-15 \le h \le 15$	$-14 \le h \le 15$	$-28 \le h \le 27$
	$-39 \le k \le 30$	$-20 \le k \le 21$	$-14 \le k \le 14$
	$-42 \le l \le 43$	$-24 \le l \le 24$	$-36 \le l \le 26$
GOF on F^2	1.024	1.018	1.029
R_1,[a] wR_2[b] [$I > 2\sigma(I)$]	0.0750, 0.1914	0.1062, 0.2548	0.0325, 0.0762
R_1,[a] wR_2[b] [all data]	0.1012, 0.2043	0.2012, 0.3116	0.0364, 0.0780

[a] $R_1 = \Sigma||F_o| - |F_c||/\Sigma|F_o|$. [b] $wR_2 = [\Sigma w(F_o^2 - F_c^2)^2/\Sigma w(F_o^2)^2]^{1/2}$, $w = 1/[\sigma^2(F_o^2) + (xP)^2 + yP]$, and $P = (F_o^2 + 2F_c^2)/3$, where $x = 0.0962$ and $y = 1384.6708$ for **1**, $x = 0.1602$ and $y = 0.0000$ for **2**, and $x = 0.0361$ and $y = 201.3238$ for **3**.

$H_{56}Cd_6K_8O_{96}Si_2W_{18}$ (**3**): Cd 11.35 (11.24), K 5.26 (5.37), Si 0.94 (1.00), W 55.66 (55.48). IR (KBr pellet): 3460(s), 1624(m), 944(s), 890(s), 829(s), 775(s), 722(s), 530(m), 484(m) cm^{-1}.

X-ray Crystallography. A good-quality single-crystal with dimensions of 0.34 × 0.26 × 0.13 mm^3 for **1**, 0.14 × 0.09 × 0.07 mm^3 for **2**, and 0.37 × 0.17 × 0.12 mm^3 for **3** was mounted on a glass fiber. Intensity data were collected on a Bruker APEX-II CCD detector at 296(2) K with Mo Kα radiation (λ = 0.71073 Å). Direct methods were used to solve the structures and to locate the heavy atoms using the SHELXTL-97 program package.[8] The remaining atoms were found from successive full-matrix least-squares refinements on F^2 and Fourier syntheses. Lorentz polarization and empirical absorption corrections were applied. All the non-hydrogen atoms were refined anisotropically. Those hydrogen atoms attached to water molecules were not located. In **1**, the Co4, Co5, Co6, Co7, Co8, and Co9 positions are simultaneously statistically occupied by Co^{II} and W^{VI} elements with half occupancy for each, resulting in one expected Co^{II} ion per Keggin cage based on the charge balance and crystallographic considerations, which is not uncommon in POM chemistry.[5,7p,9a] In **2**, the W12, W13, W14, W15, W16, and W17 atoms are disordered over two positions with the site occupancy of 0.5. This disorder phenomenon in **2** is the same as that in $[Mn(H_2O)_2\{Mn_3(B\text{-}\beta\text{-}GeW_9O_{33}(OH))(B\text{-}\beta\text{-}GeW_8O_{30}(OH))\}_2]^{22-}$.[2m] The very large solvent accessible voids in the solid-state structures of **1** and **2** may be related to the fact that it is very difficult for large molecules to adopt the most close arrangenment when they form the crystals. This phenomenon has been previously oberved.[2m,9b] Crystallographic data and structure refinements for **1**−**3** were summarized in Table 1. Further details of the crystal structures for **1**, **2**, and **3** may be obtained from the Fachinformationszentrum Karlsruhe, 76344 Eggenstein-Leopoldshafen, Germany (fax: (+49)7247-808-666; e-mail: crystdata@fiz-karlsruhe.de) on quoting the depository numbers CSD-422502 (**1**), CSD-422503 (**2**), and CSD-422504 (**3**).

RESULTS AND DISCUSSION

Synthesis. In the previously reported studies, the molar ratios of TM cations/dilacunary Keggin precursors in the reaction are mostly lower than 5; moreover, the reactions of dilacunary Keggin $K_8[\gamma\text{-}GeW_{10}O_{36}]\cdot 6H_2O$ and $K_8[\gamma\text{-}SiW_{10}O_{36}]\cdot 12H_2O$ precursors with TM cations are mostly performed in the buffer solution on heating (vide supra).[2m,4b,7b,7d,7e,7i,7k,7m] The buffer solution is often employed, which may be related to the case that the precursors are anticipated to be retained in the buffer system. Although the buffer system is utilized, they still do not preclude the precursors from transforming other POM units. Table 2 summarizes synthetic conditions, related products, and transformations between different POM units in the documents (Figure 1) and this work. However, the exploration on the interactions of two precursors and TM cations with the molar ratios of TM cations/dilacunary Keggin precursors being higher than 5 without heating is less developed.[7i,k] In this context, this work has been carried out. When $K_8[\gamma\text{-}GeW_{10}O_{36}]\cdot 6H_2O$ was used to react with $CoCl_2\cdot 6H_2O$ at room temperature in the aqueous solution, the novel trimer **1** was first isolated. Parallel experiments indicated that **1** was also formed when the molar ration of $CoCl_2\cdot 6H_2O/K_8[\gamma\text{-}GeW_{10}O_{36}]\cdot 6H_2O$ varied in the range 5−30. Because **1** contains the monovacant Keggin $[\alpha\text{-}GeW_{11}O_{38}]^{6-}$ fragments, the precursor $[\alpha\text{-}GeW_{11}O_{39}]^{8-}$ was used to react with $CoCl_2\cdot 6H_2O$ under similar conditions; unluckily, we failed to obtain **1**. In addition, the trimeric aggregate $[Rb\subset(GeW_{10}Mn_2O_{38})_3]^{17-}$ was also prepared by $K_8[\gamma\text{-}GeW_{10}O_{36}]\cdot 6H_2O$.[5] Considering the influence of different TM ions on structural diversity, when $Fe_2(SO_4)_3$ was introduced, unexpectedly, a trinuclear iron sulfate cluster $K_2(H_3O)_3[Fe_3(H_2O)_3O(SO_4)_6]\cdot 6H_2O$ was afforded.[11] Under similar

dx.doi.org/10.1021/cg200077r |Cryst. Growth Des. 2011, 11, 1913–1923

Table 2. Summary of Synthetic Conditions, Related Phases, and Transformations between Different POM Units

molar ratio of the TM cation and the precursor	T (°C)	synthetic method	reaction system	phase and transformation
$Fe^{3+}/[\gamma\text{-}GeW_{10}O_{36}]^{8-}$ = 1.118/1	40	solvent evaporation	HAc/KAc buffer	$[K(H_2O)(\beta\text{-}Fe_2GeW_{10}O_{37}(OH))(\gamma\text{-}GeW_{10}O_{36})]^{12-}$ [4b] (Figure 1a,1b)
$Fe^{3+}/[\gamma\text{-}GeW_{10}O_{36}]^{8-}$ = 2.176/1	45	solvent evaporation	HAc/KAc buffer	$[\{\beta\text{-}Fe_2GeW_{10}O_{37}(OH)_2\}_2]^{12-}$ [4b] (Figure 1b)
$Cu^{2+}/[\gamma\text{-}GeW_{10}O_{36}]^{8-}$ = 1.647/1	50	solvent evaporation	HAc/KAc buffer	$[Cu_3(H_2O)(B\text{-}\beta\text{-}GeW_9O_{33}(OH))(B\text{-}\beta\text{-}GeW_8O_{30}(OH))]^{12-}$ [2m] (Figure 1c,1d)
$Co^{2+}/[\gamma\text{-}GeW_{10}O_{36}]^{8-}$ = 1.647/1	50	solvent evaporation	HAc/KAc buffer	$[Co(H_2O)_2\{Co_3(B\text{-}\beta\text{-}GeW_9O_{33}(OH))(B\text{-}\beta\text{-}GeW_8O_{30}(OH))\}_2]^{22-}$ [2m] (Figure 1c, 1d)
$Mn^{2+}/[\gamma\text{-}GeW_{10}O_{36}]^{8-}$ = 1.647/1	60	solvent evaporation	HAc/KAc buffer	$[Mn(H_2O)_2\{Mn_3(B\text{-}\beta\text{-}GeW_9O_{33}(OH))(B\text{-}\beta\text{-}GeW_8O_{30}(OH))\}_2]^{22-}$ [2m] (Figure 1c, 1d)
$Mn^{2+}/[\gamma\text{-}GeW_{10}O_{36}]^{8-}$ = 1.600/1	room temp	solvent evaporation	aqueous solution	$[Rb\subset(GeW_{10}Mn_2O_{38})_3]^{17-}$ [5] (Figure 1a)
$Co^{2+}/[\gamma\text{-}GeW_{10}O_{36}]^{8-}$ = 19.704/1	room temp	solvent evaporation	aqueous solution	**1** (Figure 1e)
$Mn^{2+}/[\gamma\text{-}SiW_{10}O_{36}]^{8-}$ = 1.600/1	room temp	solvent evaporation	CH_3CN/water	$[(CH_3)_3(C_6H_5)N]_4[(SiO_4)W_{10}Mn^{III}_2O_{36}H_6]\cdot 2CH_3CN\cdot H_2O$ [7a] (Figure 1a)
$Cr^{3+}/[\gamma\text{-}SiW_{10}O_{36}]^{8-}$ = 2.394/1	80	solvent evaporation	HAc/KAc buffer	$[\gamma\text{-}SiO_4W_{10}O_{32}(OH)Cr_2(OOCCH_3)_2(OH_2)_2]$ [7b] (Figure 1a)
$Ni^{2+}/[\gamma\text{-}SiW_{10}O_{36}]^{8-}$ = 2.280/1	50	solvent evaporation	HAc/KAc buffer	$[\{\beta\text{-}SiNi_2W_{10}O_{36}(OH)_2(H_2O)\}_2]^{12-}$ [7d] (Figure 1b)
$M^{2+}/[\gamma\text{-}SiW_{10}O_{36}]^{8-}$ = 3.000/1 (M = Mn, Cu, Zn)	90	solvent evaporation	HAc/NaAc buffer	$[\{SiM_2W_9O_{34}(H_2O)\}_2]^{12-}$ (M = Cu^{II}, Mn^{II}, Zn^{II}) [7e] (Figure 1f)
$Mn^{2+}/[\gamma\text{-}SiW_{10}O_{36}]^{8-}$ = 3.000/1	room temp	solvent evaporation	aqueous solution	$[(\beta_2\text{-}SiW_{11}MnO_{38}OH)_3]^{15-}$ [7f] (Figure 1g)
$Ti^{4+}/[\gamma\text{-}SiW_{10}O_{36}]^{8-}$ = 2.200/1	80	solvent evaporation	aqueous solution	$[\{\beta\text{-}Ti_2SiW_{10}O_{39}\}_4]^{24-}$ [7g] (Figure 1b)
$Co^{2+}/[\gamma\text{-}SiW_{10}O_{36}]^{8-}$ = 13.194/1	50	solvent evaporation	NaCl aqueous solution	$[Co_6(H_2O)_{30}\{Co_9Cl_2(OH)_3(H_2O)_9(\beta\text{-}SiW_8O_{31})_3\}]^{5-}$ [7i] (Figure 1d)
$Co^{2+}/[\gamma\text{-}SiW_{10}O_{36}]^{8-}$ = 2.194/1	50	solvent evaporation	HAc/NaAc buffer	$[\{Co_3(B\text{-}\beta\text{-}SiW_9O_{33}(OH))(B\text{-}\beta\text{-}SiW_8O_{29}(OH)_2)\}_2]^{22-}$ [7j] (Figure 1c, 1d)
$Zr^{4+}/[\gamma\text{-}SiW_{10}O_{36}]^{8-}$ = 8.778/1	50	solvent evaporation	HAc/KAc buffer	$[Zr_6O_2(OH)_4(H_2O)_3(\beta\text{-}SiW_{10}O_{37})_3]^{14-}$ [7k] (Figure 1b)
$Zr^{4+}/[\gamma\text{-}SiW_{10}O_{36}]^{8-}$ = 4.389/1	50	solvent evaporation	HAc/KAc buffer	$[Zr_4O_2(OH)_2(H_2O)_4(\beta\text{-}SiW_{10}O_{37})_2]^{10-}$ [7k] (Figure 1b)
$Fe^{3+}/[\gamma\text{-}SiW_{10}O_{36}]^{8-}$ = 2.030/1	room temp	solvent evaporation	aqueous solution	$[\{Fe_2(OH)_3(H_2O)_2\}_3(\gamma\text{-}SiW_{10}O_{36})_3]^{15-}$ [7l] (Figure 1a)
$Fe^{3+}/[\gamma\text{-}SiW_{10}O_{36}]^{8-}$ = 2.030/1	room temp	solvent evaporation	HAc/KAc buffer	$[\{Fe(OH)(OAc)\}_4(\gamma\text{-}SiW_{10}O_{36})_2]^{12-}$ [7m] (Figure 1a)
$Mn^{2+}/[\gamma\text{-}SiW_{10}O_{36}]^{8-}$ = 1.993/1	room temp	solvent evaporation	methanol−acetonitrile solution	$[\{(\gamma\text{-}SiW_{10}O_{36})Mn_2(OH)_2(N_3)_{0.5}(H_2O)_{0.5}\}_2(\mu\text{-}1,3\text{-}N_3)]^{10-}$ [7n] (Figure 1a)
$Cu^{2+}/[\gamma\text{-}SiW_{10}O_{36}]^{8-}$ = 1.993/1	room temp	solvent evaporation	methanol−acetonitrile solution	$[(\gamma\text{-}SiW_{10}O_{36})_2Cu_4(\mu\text{-}1,1,1\text{-}N_3)_2(\mu\text{-}1,1,1\text{-}N_3)_2]^{12-}$ [7n] (Figure 1a)
$Co^{2+}/[\gamma\text{-}SiW_{10}O_{36}]^{8-}$ = 2.077/1	room temp	solvent evaporation	aqueous solution	$[\{(B\text{-}\beta\text{-}SiW_9O_{33}(OH))(\beta\text{-}SiW_8O_{29}(OH)_2)Co_3(H_2O)\}_2Co(H_2O)_2]^{20-}$ [7o] (Figure 1c, 1d)
$Ni^{2+}/[\gamma\text{-}SiW_{10}O_{36}]^{8-}$ = 6.818/1	100	hydrothermal conditions	aqueous solution	$\{[Ni(dap)_2(H_2O)]_2[Ni(dap)_2]_2[Ni_4(Hdap)_2(\alpha\text{-}B\text{-}HSiW_9O_{34})_2]\}\cdot 7H_2O$ [2j] (Figure 1f)
$Cu^{2+}/[\gamma\text{-}SiW_{10}O_{36}]^{8-}$ = 15.000/1	100	hydrothermal conditions	aqueous solution	$\{[Cu(en)_2(H_2O)]_2[Cu(en)_2][\alpha\text{-}SiCuW_{11}O_{39}]\}\cdot 5H_2O$ [7p] (Figure 1e)
$Mn^{2+}/[\gamma\text{-}SiW_{10}O_{36}]^{8-}$ = 5.112/1	room temp	solvent evaporation	HAc/NaAc buffer	**2** (Figure 1c, 1d)
$Cd^{2+}/[\gamma\text{-}SiW_{10}O_{36}]^{8-}$ = 10.337/1	room temp	solvent evaporation	HAc/NaAc buffer	**3** (Figure 1f)

dx.doi.org/10.1021/cg200077t|Cryst. Growth Des. 2011, 11, 1913–1923

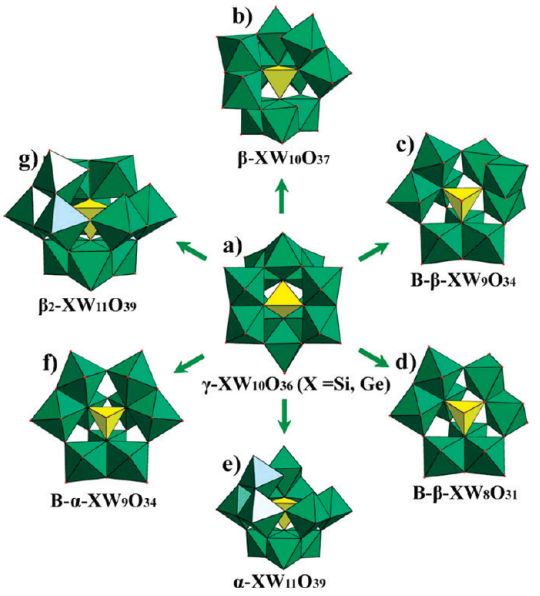

Figure 1. Transformations between γ-$XW_{10}O_{36}$ and different POM units.

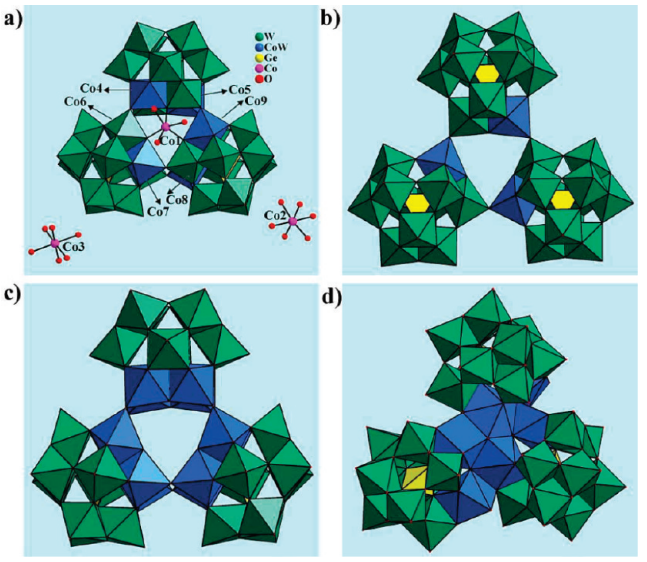

Figure 2. (a) Combined ball-and-stick/polyhedral representation of **1a** with selected numbering scheme. (b) View of **A**.[7f] (c) View of **B**.[5] The Rb^+ cation is omitted for clarity. (d) View of $[Zr_6O_2(OH)_4(H_2O)_3(\beta\text{-}SiW_{10}O_{37})_3]^{14-}$.[7k]

conditions to **1**, the replacement of $CoCl_2\cdot 6H_2O$ with $MnCl_2\cdot 4H_2O$ led to the formation of the reported $[Mn(H_2O)_2\{Mn_3(B\text{-}\beta\text{-}GeW_9O_{33}(OH))(B\text{-}\beta\text{-}GeW_8O_{30}(OH))\}_2]^{22-}$,[2m] whose structure somewhat resembles **2**. When replacing the Co^{II} ion with Fe^{II}, Ni^{II}, Cu^{II}, Zn^{II}, and Cd^{II} ions, only amorphous powders were obtained. Currently, we are intensively exploring this system by controlling reaction conditions with the aim of finding much more TMSP species. During the course of exploiting the reaction of $K_8[\gamma\text{-}GeW_{10}O_{36}]\cdot 6H_2O$ with TM ions, the interaction of $K_8[\gamma\text{-}SiW_{10}O_{36}]\cdot 12H_2O$ with TM cations in the HAc/NaAc buffer was being simultaneously performed. When the molar ratio of $CoCl_2\cdot 6H_2O/K_8[\gamma\text{-}SiW_{10}O_{36}]\cdot 12H_2O$ varied in the range 10−20, a reported 15-cobalt-substituted TMSP $[Co_6(H_2O)_{30}\{Co_9Cl_2(OH)_3(H_2O)_9(\beta\text{-}SiW_8O_{31})_3\}]^{5-}$ was obtained.[7i] When $MnCl_2\cdot 4H_2O$ replaced $CoCl_2\cdot 6H_2O$ and the molar ratio of $MnCl_2\cdot 4H_2O/K_8[\gamma\text{-}SiW_{10}O_{36}]\cdot 12H_2O$ was changed to 5−7, **2** was harvested, which is a one-dimensional chain built by rare tetrameric $\{[Mn(H_2O)_3]_2[Mn(H_2O)_2][(B\text{-}\beta\text{-}SiW_9O_{34})Mn_3(H_2O)(B\text{-}\beta\text{-}SiW_8O_{31})]_2\}^{22-}$ units. When $3CdSO_4\cdot 8H_2O$ was employed, the two-dimensional sandwich-type silicotungstate **3** was isolated. Parallel experiments showed that **3** can not be synthesized by reaction of the precursor $[\alpha\text{-}SiW_9O_{34}]^{10-}$ with $3CdSO_4\cdot 8H_2O$. Actually, to date, the reported tetra-TM substituted sandwich-type silicotungstates $[M_4(H_2O)_2(B\text{-}\alpha\text{-}SiW_9O_{34})_2]^{12-}$ (M = Mn^{II}, Cu^{II}, Zn^{II}),[7e] $\{[Ni(dap)_2(H_2O)]_2[Ni(dap)_2]_2[Ni_4(Hdap)_2(B\text{-}\alpha\text{-}HSiW_9O_{34})_2]\}\cdot 7H_2O$,[2j] and $Na_4[Mn_4(H_2O)_{18}Mn_4(H_2O)_2(SiW_9O_{34})_2]\cdot 22H_2O$[10] were all made by means of $K_8[\gamma\text{-}SiW_{10}O_{36}]\cdot 12H_2O$. These results showed that the transformation of $[\gamma\text{-}SiW_{10}O_{36}]^{8-}$ to $[B\text{-}\alpha\text{-}SiW_9O_{34}]^{10-}$ is indispensable in the formation of these sandwich-type silicotungstates. Presently, the reactions of Fe^{II}, Ni^{II}, Cu^{II}, and Zn^{II} ions with $K_8[\gamma\text{-}SiW_{10}O_{36}]\cdot 12H_2O$ are in progress. As discussed above, comparison of the reactions of two dilacunary precursors with TM cations illustrated that the inherent essentiality of two dilacunary precursors and the nature of TM cations can all affect the structural types of the product phases. In fact, although the structures of $[\gamma\text{-}GeW_{10}O_{36}]^{8-}$ and $[\gamma\text{-}SiW_{10}O_{36}]^{8-}$ are almost isostructural, both reaction behaviors are rather different, which may be related to the discrepancy of the heteroatom in the $[\gamma\text{-}XW_{10}O_{36}]^{8-}$ unit (X = Ge^{IV}, Si^{IV}). These have been supported by a large number of Kortz's findings.[2m,4b,7d−7g,7i−7k] For example, the interactions of $[\gamma\text{-}GeW_{10}O_{36}]^{8-}$ with Cu^{II}, Co^{II}, and Mn^{II} cations led to the TMSPs with mixed POM fragments $[Cu_3(H_2O)(B\text{-}\beta\text{-}GeW_9O_{33}(OH))(B\text{-}\beta\text{-}GeW_8O_{30}(OH))]^{12-}$,[2m] and $[M(H_2O)_2\{M_3(B\text{-}\beta\text{-}GeW_9O_{33}(OH))(B\text{-}\beta\text{-}GeW_8O_{30}(OH))\}_2]^{22-}$ (M = Co^{II}, Mn^{II}),[2m] in contrast, when $[\gamma\text{-}SiW_{10}O_{36}]^{8-}$ was reacted with Cu^{II}, Co^{II}, and Mn^{II} cations, giving rise to the tetra-TM sandwiched silicotungstates $[\{SiM_2W_9O_{34}(H_2O)\}_2]^{12-}$ (M = Cu^{II}, Mn^{II}), with identical POM fragments[7e] and the tri-Co^{II} sandwiched dimer $[\{Co_3(B\text{-}\beta\text{-}SiW_9O_{33}(OH))(B\text{-}\beta\text{-}SiW_8O_{29}(OH)_2)\}_2]^{22-}$ with mixed POM fragments.[7j] In short, both previous studies and our work indicate that the nature of TM cations mainly influences the structural architectures of the products when the dilacunary precursors are the same whereas the discrepancy of the heteroatom in the $[\gamma\text{-}XW_{10}O_{36}]^{8-}$ unit chiefly produces an effect on the structural diversity of the products when TM cations are identical. It should be noted that the isolation of **1**−**3** illustrates that the anticonventional thinking is effective and feasible in the preparation of novel TMSPs. However, this approach still needs to be further explored, because many factors (the pH of the solution, the nature of the metal ions, the temperature and the concentration of the reaction mixture, *etc.*) can affect the formation of crystal phases and the structural variety of the products. Thus, lanthanide cations and 3d-4f heterometal cations will be introduced in due time. We believe that much more novel TMSPs with unexpected structures should be separated in the following period.

On the other hand, structural transformations between $[\gamma\text{-}XW_{10}O_{36}]^{8-}$ (X = Ge^{IV}, Si^{IV}) and other POM units in this work have been observed (Figure 1). In the preparation of **1**, the conversion of $[\gamma\text{-}GeW_{10}O_{36}]^{8-}$ to $[\alpha\text{-}GeW_{11}O_{39}]^{8-}$ has taken place (Figure 1a → 1e). Similar conversion of $[\gamma\text{-}SiW_{10}O_{36}]^{8-}$ to $[\alpha\text{-}SiW_{11}O_{39}]^{8-}$ has also been encountered by us.[7p] In the formation of **2**, the simultaneous transformations of $[\gamma\text{-}SiW_{10}O_{36}]^{8-}$ to

$[B\text{-}\beta\text{-}SiW_9O_{34}]^{10-}$ and $[B\text{-}\beta\text{-}SiW_8O_{31}]^{10-}$ have occurred (Figure 1a → 1c and 1a → 1d). Such a phenomenon has been observed by Kortz[7j] and Mialane.[7o] Recently, Kortz et al. have discovered that $[\gamma\text{-}GeW_{10}O_{36}]^{8-}$ can also change to $[B\text{-}\beta\text{-}GeW_9O_{34}]^{10-}$ and $[B\text{-}\beta\text{-}GeW_8O_{31}]^{10-}$.[2m] Besides the above isomerization of $[\gamma\text{-}SiW_{10}O_{36}]^{8-}$ to $[B\text{-}\beta\text{-}SiW_9O_{34}]^{10-}$, we have observed that $[\gamma\text{-}SiW_{10}O_{36}]^{8-}$ can isomerize to $[B\text{-}\alpha\text{-}SiW_9O_{34}]^{10-}$ in the synthesis of **3** (Figure 1a → 1f). Furthermore, the isomerizations of $[\gamma\text{-}SiW_{10}O_{36}]^{8-}$ to $[B\text{-}\alpha\text{-}SiW_9O_{34}]^{10-}$ in the conventional aqueous solution or under hydrothermal conditions have been encountered.[7e,2j] These phenomena further consolidate that the dilacunary Keggin precursors $[\gamma\text{-}XW_{10}O_{36}]^{8-}$ are metastable and labile and can transform to different POM frameworks and isomerize to the α- and β-configurations.

Structural Descriptions. The molecular structure of **1** consists of a cyclic trimeric $[Co(H_2O)_3(\alpha\text{-}GeW_{11}CoO_{38})_3]^{10-}$ polyoxoanion (**1a**), two discrete $[Co(H_2O)_6]^{2+}$ cations, three Cs^+ cations, three K^+ cations, and 30 lattice water moelcules (Figure 2a). Interestingly, **1a** is novel, although two simialr trimeric cyclic polyoxoanions $[(\beta_2\text{-}SiW_{11}MnO_{38}OH)_3]^{15-}$ (**A**) (Figure 2b)[7f] and $[Rb\subset(GeW_{10}Mn_2O_{38})_3]^{17-}$ (**B**) (Figure 2c)[5] have already been reported. **1a** is constructed from three corner-sharing monocobalt substituted Keggin $[\alpha\text{-}GeW_{11}CoO_{38}]^{4-}$ units linked together via six Co/W−O−W connectivities; meanwhile, three monocobalt substituted α-Keggin units are also combined with each other through an anchoring octahedral $[Co1(H_2O)_3]^{2+}$ cation coordinating to three bridging oxygen atoms on three $[\alpha\text{-}GeW_{10}Mn_2O_{38}]^{4-}$ units [Co1−O_b: 2.136(16)−2.192(18) Å; Co1−O_W: 2.07(3)−2.15(2) Å]. In **1a**, the Co4, Co5, Co6, Co7, Co8, and Co9 positions are simultaneously statistically occupied by Co^{II} and W^{VI} elements with half occupancy for each, resulting in one expected Co^{II} ion per Keggin cage, and this similarly disordered phenomenon is also observed in **A**[7f] and **B**.[5] Furthermore, the Co/W−O−W angles between adjacent Keggin units are in the range 127.1(10)−132.6(10)°, being smaller than the Mn−O−W angles (145°) in **A**[7f] and the Mn−O−W angles (134−136°) in **B**,[5] the main reason of which may be related to the anchoring $[Co1(H_2O)_3]^{2+}$ cation covalently connecting three α-Keggin $[\alpha\text{-}GeW_{10}Mn_2O_{38}]^{4-}$ units. In comparison with the reported **A**[7f] and **B**,[5] three common features are observed: (a) three TMSPs are all prepared by reaction of divacant Keggin precursors with TM cations; (b) all display the trimeric cyclic structures; (c) those TM cations encapsulated into the defect sites of lacunary Keggin moieties are all disordered. The major discrepancies between **1a** and **A**[7f] are as follows: (a) the configuration of the Keggin units in the former is α-type whereas that in the latter is β_2-type; (b) in the fomer, three monocobalt substituted Keggin units are combined together via six Co/W−O−W connectivities and a $[Co(H_2O)_3]^{2+}$ bridge while, in the latter, three monomanganese substituted Keggin units are joined together only via three Mn/W−O−W linkers. The obvious difference between **1a** and **B**[5] is that a capping $[Co(H_2O)_3]^{2+}$ cation participates in a combination of three monocobalt substituted Keggin units. In addition, a novel asymmetric hexa-zirconium substituted trimer $[Zr_6O_2(OH)_4(H_2O)_3(\beta\text{-}SiW_{10}O_{37})_3]^{14-}$ has been reported by Kortz et al.[7k]

The molecular structural unit of **2** is composed of a rare centric tetrameric $\{[Mn(H_2O)_3]_2[Mn(H_2O)_2][(B\text{-}\beta\text{-}SiW_9O_{33}(OH))Mn_3(H_2O)(B\text{-}\beta\text{-}SiW_8O_{30}(OH))]_2\}^{18-}$ (**2a**) subunit (Figure 3a), 18 K^+ counter cations, and 16 lattice water molecules. The structure of **2a** is very interesting and constructed from two structurally equivalent asymmetric sandwich-type $[(B\text{-}\beta\text{-}SiW_9O_{33}(OH))Mn_3(H_2O)(B\text{-}\beta\text{-}SiW_8O_{30}(OH))]^{12-}$ moieties (Figure 3b) held together by two structurally equivalent $[Mn(H_2O)_3]^{2+}$ cations

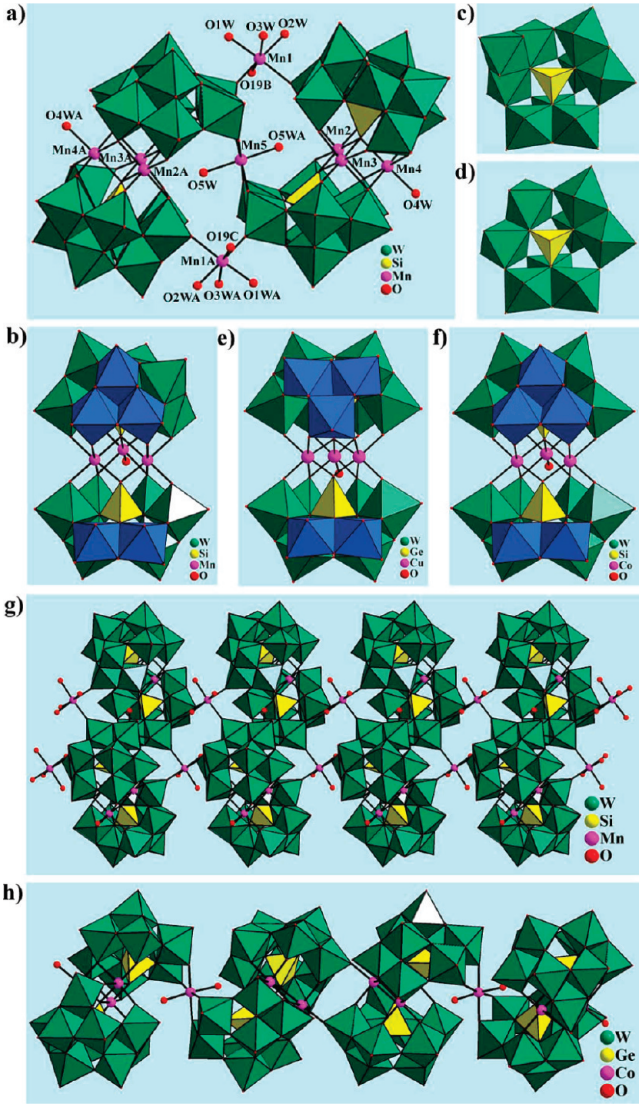

Figure 3. (a) Combined ball-and-stick/polyhedral representation of **2a** with selected numbering scheme. The atoms with "A, B, C" in their labels are symmetrically generated (A: $2-x, 2-y, -z$; B: $-1+x, y, z$; C: $3-x, 2-y, -z$). (b) Combined ball-and-stick/polyhedral representation of the $[(B\text{-}\beta\text{-}SiW_9O_{33}(OH))Mn_3(H_2O)(B\text{-}\beta\text{-}SiW_8O_{30}(OH))]^{12-}$ moiety in **2a**. (c) View of the trilacunary Keggin $[B\text{-}\beta\text{-}SiW_9O_{34}]^{10-}$ fragment. (d) View of the dilacunary Keggin $[B\text{-}\beta\text{-}SiW_8O_{31}]^{10-}$ fragment. (e) Combined ball-and-stick/polyhedral view of **G**.[2m] (f) Combined ball-and-stick/polyhedral view of $[Co_3(H_2O)(B\text{-}\alpha\text{-}SiW_9O_{34})(B\text{-}\beta\text{-}SiW_8O_{31})]^{14-}$.[11] (g) The one-dimensional chain built by **2a** subunits. (h) The one-dimensional chain formed by $[Co(H_2O)_2\{Co_3(B\text{-}\beta\text{-}GeW_9O_{33}(OH))(B\text{-}\beta\text{-}GeW_8O_{30}(OH))\}_2]^{22-}$ subunits.[2m].

[Mn−O: 2.09(3)−2.26(3) Å] and a unique $[Mn(H_2O)_2]^{2+}$ cation [Mn−O: 2.09(3)−2.23(3) Å]. Notably, the structure of **2a** is distinguished from that of the reported $[Mn(H_2O)_2\{Mn_3(B\text{-}\beta\text{-}GeW_9O_{33}(OH))(B\text{-}\beta\text{-}GeW_8O_{30}(OH))\}_2]^{22-}$ (**C**)[2m] and their key difference is that two asymmetric sandwich-type moieties in **2a** are combined with each other by two $[Mn(H_2O)_3]^{2+}$ and a $[Mn(H_2O)_2]^{2+}$ bridge while two asymmetric sandwich-type moieties in **C**[2m] are linked together through only one $[Mn(H_2O)_2]^{2+}$ bridge. The asymmetric sandwich-type $[(B\text{-}\beta\text{-}SiW_9O_{33}(OH))Mn_3(H_2O)(B\text{-}\beta\text{-}SiW_8O_{30}(OH))]^{12-}$ moiety in **2a** is built up of three

manganese ions [Mn−O: 2.07(3)−2.27(3) Å] encapsulated by two unequivalent lacunary Keggin fragments $[B\text{-}\beta\text{-}SiW_9O_{34}]^{10-}$ (Figure 3c) and $[B\text{-}\beta\text{-}SiW_8O_{31}]^{10-}$ (Figure 3d). Therefore, the formation of **2** must involve rotational isomerization of $[\gamma\text{-}SiW_{10}O_{36}]^{8-}$ ($\gamma \rightarrow \beta$ lacunary Keggin) followed by loss of tungsten ($[\gamma\text{-}SiW_{10}O_{36}]^{8-} \rightarrow [B\text{-}\beta\text{-}SiW_9O_{34}]^{10-} \rightarrow [B\text{-}\beta\text{-}SiW_8O_{31}]^{10-}$) followed by manganese insertion. The same transformation was already discussed by Cronin et al. in 2008.[11] A similar process on germantungstates was also observed by Kortz et al. in 2009.[2m] In fact, the $[B\text{-}\beta\text{-}SiW_9O_{34}]^{10-}$ fragment was for the first time observed by Kortz et al. in a cobalt-containing silicotungstate sandwich-type dimer $[\{Co_3(B\text{-}\beta\text{-}SiW_9O_{33}(OH))(B\text{-}\beta\text{-}SiW_8O_{29}(OH)_2)\}_2]^{22-}$ (**D**).[7j] Moreover, the $[B\text{-}\beta\text{-}SiW_8O_{31}]^{10-}$ fragment was also first discovered by Kortz et al. in a satellite-shaped 15-Co polyoxotungstate $[Co_6(H_2O)_{30}\{Co_9Cl_2(OH)_3(H_2O)_9(\beta\text{-}SiW_8O_{31})_3\}]^{5-}$ (**E**).[7i] The asymmetric sandwich-type structural type containing $[B\text{-}\beta\text{-}XW_9O_{34}]^{10-}$ and $[B\text{-}\beta\text{-}XW_8O_{31}]^{10-}$ (X = Si^{IV}, Ge^{IV}) fragments held together by three TM ions in **2a** was encountered in several polyoxotungstates **D**,[7j] $[Co_3(H_2O)(B\text{-}\beta\text{-}SiW_9O_{34})(B\text{-}\beta\text{-}SiW_8O_{29}(OH)_2)]^{12-}$ (**F**),[11] $[Cu_3(H_2O)(B\text{-}\beta\text{-}GeW_9O_{33}(OH))(B\text{-}\beta\text{-}GeW_8O_{30}(OH))]^{12-}$ (**G**),[2m] $[Co(H_2O)_2\{Co_3(B\text{-}\beta\text{-}GeW_9O_{33}(OH))(B\text{-}\beta\text{-}GeW_8O_{30}(OH))\}_2]^{22-}$ (**H**),[2m] and **C**.[2m] More intriguingly, a close inspection indicates that asymmetric sandwich-type moieties in **2a**, **D**,[7j] **F**,[11] **H**,[2m] **C**,[2m] and **G**[2m] are somewhat different, although they all consist of the same Keggin fragments. The asymmetric sandwich-type moieties with C_1 symmetry in **2a**, **D**,[7j] **F**,[11] **H**,[2m] and **C**[2m] lack a plane of symmetry due to the positioning of the rotated triad "on the side" of the moieties (Figure 3b) whereas the asymmetric sandwich-type moiety with C_s symmetry in **G** has a plane of symmetry which passes through the rotated triad of the $[B\text{-}\beta\text{-}GeW_9O_{34}]^{10-}$ fragment (Figure 3e), which was first observed by Kortz et al.[2m] The reason for differences of the asymmetric sandwich-type moieties in **2a**, **D**,[7j] **F**,[11] **H**,[2m] **C**,[2m] and **G**[2m] may be related to the different electron configurations and coordination geometries of TM cations.[2m] On the other hand, another asymmetric sandwich-type structural type with C_s symmetry containing $[B\text{-}\alpha\text{-}SiW_9O_{34}]^{10-}$ and $[B\text{-}\beta\text{-}SiW_8O_{31}]^{10-}$ fragments connected together by three cobalt ions (Figure 3f) has been discovered by Cronin et al. in $[Co_3(H_2O)(B\text{-}\alpha\text{-}SiW_9O_{34})(B\text{-}\beta\text{-}SiW_8O_{31})]^{14-}$.[11]

The most remarkable feature of **2** is that adjacent rare centric tetrameric **2a** subunits are linked via two equivalent $[Mn(H_2O)_3]^{2+}$ cations constructing the infinite one-dimensional chain architecture (Figure 3g), which is distinct from the one-dimensional chain structure in **F** (Figure 3h). The major differences are that their structural units and the linking modes of the one-dimensional chains are distinct. As far as we know, **2** represents the first one-dimensional silicotungstate containing asymmetric sandwich-type moieties constructed from $[B\text{-}\beta\text{-}SiW_9O_{34}]^{10-}$ and $[B\text{-}\beta\text{-}SiW_8O_{31}]^{10-}$ fragments.

The structural unit of **3** contains a two-supporting $\{[Cd(H_2O)_3]_2[Cd_4(H_2O)_2(B\text{-}\alpha\text{-}SiW_9O_{34})_2]\}^{8-}$ subunit (**3a**), 8 K^+ counter cations, and 20 lattice water molecules (Figure 4a). The centric **3a** subunit consists of a tetra-Cd^{II} sandwiched $[Cd_4(H_2O)_2(B\text{-}\alpha\text{-}SiW_9O_{34})_2]^{12-}$ core and two supporting $[Cd(H_2O)_3]^{2+}$ cations. Alternatively, **3a** can also be viewed as a fusion of two half-units with the hypothetical formula $\{[Cd(H_2O)_3][Cd_2(H_2O)(B\text{-}\alpha\text{-}SiW_9O_{34})]\}^{4-}$ related by an inversion center (0.75,0.75,0.5). The dimeric $[Cd_4(H_2O)_2(B\text{-}\alpha\text{-}SiW_9O_{34})_2]^{12-}$ core has the general structure of the series $[M_4(H_2O)_2(B\text{-}\alpha\text{-}SiW_9O_{34})_2]^{12-}$ (M = Mn^{II}, Cu^{II}, Zn^{II})[7e] and is

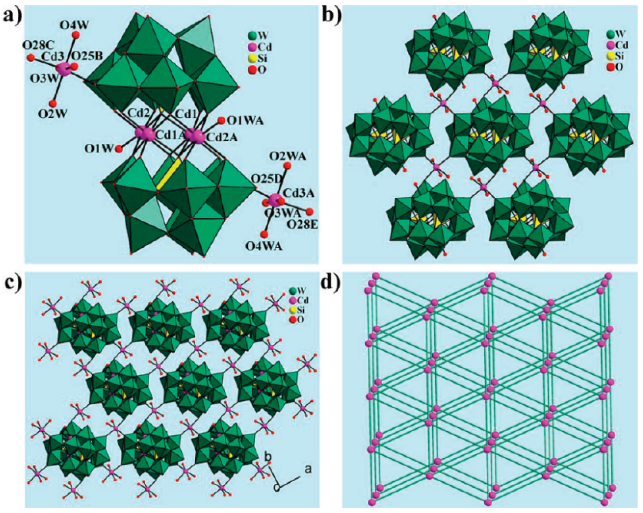

Figure 4. (a) Combined ball-and-stick/polyhedral representation of **3a** with selected numbering scheme. The atoms with "A, B, C, D, E" in their labels are symmetrically generated (A: 1.5 − *x*, 1.5 − *y*, 1 − *z*; B: 1 − *x*, 2 − *y*, 1 − *z*; C: −0.5 + *x*, −0.5 + *y*, *z*; D: 0.5 + *x*, −0.5 + *y*, *z*; E: 2 − *x*, 2 − *y*, 1 − *z*). (b) Connection between one $[Cd_4(H_2O)_2(B\text{-}\alpha\text{-}SiW_9O_{34})_2]^{12-}$ subunit and six adjacent same ones. (c) The two-dimensional sheet of **3**. (d) Topological view of the two-dimensional sheets showing the (3,6)-network and the −AAA− mode.

constructed from two trivacant Keggin $[B\text{-}\alpha\text{-}SiW_9O_{34}]^{10-}$ moieties in a staggered fashion linked via a rhomb-like Cd_4O_{16} group, resulting in a sandwich-type assembly. Specifically, the Cd_4O_{16} group is combined with two $[B\text{-}\alpha\text{-}SiW_9O_{34}]^{10-}$ fragments via exposed 14 bridging O atoms (two μ_4-O from two SiO_4 groups, four μ_3-O from four WO_6 groups, and eight μ_2-O from eight WO_6 groups). This structural type was first described by Weakley et al. for $[Co_4(H_2O)_2(PW_9O_{34})_2]^{10-}$, which is a phosphotungstate derived from the lacunary Keggin ion.[12] Both Cd1, Cd1A, Cd2, and Cd2A ions in the sandwich belt adopt the distorted octahedral geometries with the Cd−O distances of 2.210(7)−2.343(7) Å for the Cd1 ion and 2.219(7)−2.342(6) Å for the Cd2 ion. The bridging $[Cd3(H_2O)_3]^{2+}$ and $[Cd3A(H_2O)_3]^{2+}$ ions have octahedral coordination environments, in which three water oxygen atoms [Cd−O: 2.297(8)−2.329(8) Å] and one terminal oxygen atom from one adjacent $[Cd_4(H_2O)_2(B\text{-}\alpha\text{-}SiW_9O_{34})_2]^{12-}$ subunit [Cd−O: 2.257(7) Å] build the basal plane and two terminal oxygen atoms from two adjacent $[Cd_4(H_2O)_2(B\text{-}\alpha\text{-}SiW_9O_{34})_2]^{12-}$ subunits occupy two axial positions [Cd−O: 2.223(8)−2.277(7) Å].

The most intriguing beautiful feature of **3** is that each $[Cd_4(H_2O)_2(B\text{-}\alpha\text{-}SiW_9O_{34})_2]^{12-}$ subunit connects six $[Cd(H_2O)_3]^{2+}$ bridges while each $[Cd(H_2O)_3]^{2+}$ bridge links three $[Cd_4(H_2O)_2(B\text{-}\alpha\text{-}SiW_9O_{34})_2]^{12-}$ subunits (Figure 4b), resulting in an interesting two-dimensional sheet structure (Figure 4c). Notably, the construction mode of the two-dimensional sheet in **3** is remarkably different from that in the reported two-dimensional sandwich-type silicotungstate $K_3Na_5[Mn_2(H_2O)_6Mn_4(H_2O)_2(SiW_9O_{34})_2]\cdot 23.5H_2O$.[10] To our knowledge, **3** still represents the rare inorganic two-dimensional structure constructed by tetra-TM substituted sandwich-type Keggin POM units and TM bridges in the sandwich-type subfamily of POM chemistry. From the topological point of view, the two-dimensional sheet of **3** is a

dx.doi.org/10.1021/cg200077r |*Cryst. Growth Des.* 2011, 11, 1913–1923

two-dimensional (3,6) topological network, in which each $[Cd_4(H_2O)_2(B\text{-}\alpha\text{-}SiW_9O_{34})_2]^{12-}$ subunit acts as a six-connected node (Figure 4d). As far as we know, it is the first two-dimensional (3,6)-topological network in POM chemistry; albeit, several two-dimensional (4,4)-topological networks have been reported.[2j,k,13] A topological analysis of this network has been performed with OLEX.[14] The long topological (O'Keeffe) vertex symbol is $3\cdot3\cdot3\cdot3\cdot3\cdot*\cdot*\cdot*\cdot*\cdot*\cdot*\cdot*\cdot*$ for the $[Cd_4(H_2O)_2(B\text{-}\alpha\text{-}SiW_9O_{34})_2]^{12-}$ node, which gives the short vertex (Schläfli) symbol of $3^6.4^6.5^3$. Notice that adjacent layers are aligned in the −AAA− mode (Figure 4d).

IR and UV Spectra. The IR spectra of **1**−**3** display the characteristic vibration patterns derived from the Keggin POM frameworks in 600−1000 cm^{-1} (Figure S1, Supporting Information). Four characteristic bands attributable to $\nu(W-O_t)$, $\nu(X-O_a)$ (X = Ge^{IV}/Si^{IV}), $\nu(W-O_b)$, and $\nu(W-O_c)$ appear at 951, 874, 783, and 714 cm^{-1} for **1**, at 944, 905, 875, and 722 cm^{-1} for **2**, and at 944, 890, 829, and 775, 722 cm^{-1} for **3**, respectively. In comparison with the IR spectrum of $K_{8-x}Na_x[\alpha\text{-}GeW_{11}O_{39}]\cdot nH_2O$ (Figure S2, Supporting Information),[15] the split of the $\nu(W-O_b)$ vibration band in the IR spectrum of **1** disappears, which suggests that the symmetry of Keggin POM moieties remarkably increases due to the incorporation of cobalt ions to the defect sites of Keggin POM moieties.[16] In comparison with the IR spectrum of $Na_{10}[\alpha\text{-}SiW_9O_{34}]\cdot18H_2O$ (Figure S3, Supporting Information),[17] the $\nu(W-O_t)$ vibration peak for **3** has a noticeable bathochromic shift of 45 cm^{-1}, the possible reason for which may be that the charge compensation cations and bridging $[Cd(H_2O)_3]^{2+}$ cations have stronger interactions with the terminal oxygen atoms of the polyoxoanion, impairing the W−O_t bond, reducing the W−O_t bond force constant, and leading to decreasing of the W−O_t vibration frequency.[18] The $\nu(Si-O_a)$ and $\nu(W-O_b)$ vibration frequencies for **3** also have bathochromic shifts of 46 and 38 cm^{-1}, respectively, as compared to that of $Na_{10}[\alpha\text{-}SiW_9O_{34}]\cdot18H_2O$, the possible reason for which may be that the rhomb-like Cd_4O_{16} group coordinates to the lacunae of two $[B\text{-}\alpha\text{-}SiW_9O_{34}]^{10-}$ fragments. Obviously, the IR spectra of **1**, **2**, and **3** are distinct from those of the divacant precursors $[\gamma\text{-}XW_{10}O_{36}]^{8-}$ (X = Ge^{IV}, Si^{IV}) (Figure S4, Supporting Information), which further proves the transformations of $[\gamma\text{-}XW_{10}O_{36}]^{8-}$ to other Keggin fragments, being in good agreement with the results of single-crystal structural analyses. The UV−vis spectra of **1**, **2**, and **3** were recorded in aqueous solution. Only one absorption band centered at ca. 250 nm for **1**, 261 nm for **2**, and 253 nm for **3** is observed in the region of 190−400 nm, respectively (Figure S5, Supporting Information), which is assigned to the $p\pi-d\pi$ charge-transfer transitions of the $O_{b,c}\rightarrow W$ bonds.[18] The absorption band attributed to the charge-transfer transitions of the $O_t\rightarrow W$ bonds is shifted to the near UV region. In the visible region of **1** (Figure S6, Supporting Information), an absorption band at 562 nm ascribed to the Co-centered d−d transitions is also observed, being in good consistency with the reported value.[19a] However, no absorption band appears in the visible region of **2** because of the rather weak absorbance corresponding to the Mn-centered d−d transitions; this phenomenon is constantly encountered previously.[19]

Magnetic Properties. Considering the presence of the magnetic centers in **1** and **2**, both magnetic properties were investigated. The temperature dependence of the magnetic susceptibility for **1** is shown in Figure 5. The χ_M slowly increases from 0.10 emu mol^{-1} at 300 K to 0.75 emu mol^{-1} at 24 K and then exponentially reaches the maximum of

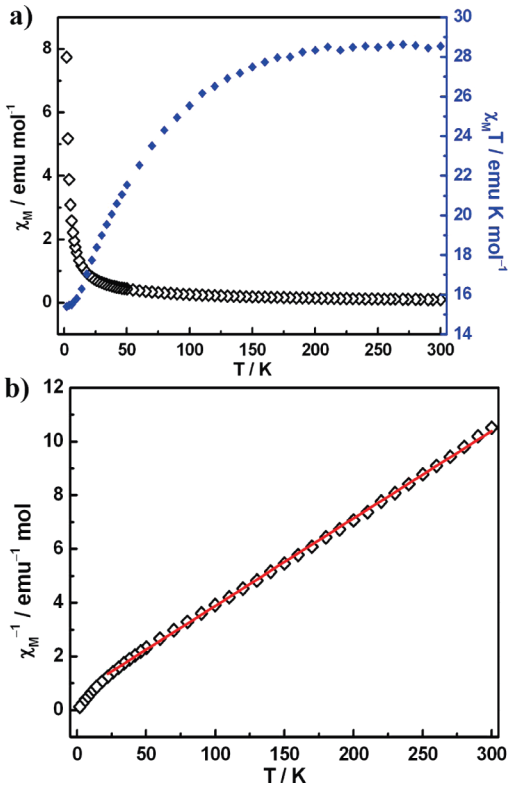

Figure 5. (a) Temperature dependence of the magnetic susceptibility for **1** between 2 and 300 K. (b) Temperature evolution of the inverse magnetic susceptibility for **1** between 24 and 300 K. The red solid line was generated from the best fit by the Curie−Weiss expression.

7.74 emu mol^{-1} at 2 K (Figure 5a). The $\chi_M T$ product at room temperature is 28.54 emu K mol^{-1}, being higher than the spin-only value (11.25 emu K mol^{-1}) for six noninteracting high-spin Co^{II} ions ($S = {}^3/_2$) with $g = 2.00$, which illustrates that there is an appreciable spin−orbit coupling expected for octahedrally coordinated Co^{II} ions.[20] The Co^{II} ions in an octahedral coordination have a high-spin ground state $^4T_1$ with first-order spin−orbit coupling. This ground state is split into six anisotropic Kramers doublets.[7o] Upon cooling, the $\chi_M T$ decreases and reaches a minimum of 15.41 emu K mol^{-1} at 2 K, indicating the antiferromagentic interactions within the Co^{II} centers. The magnetic susceptibility data between 24 and 300 K are fit to the Curie−Weiss expression, affording the Curie constant $C = 30.72$ emu K mol^{-1} and the Weiss constant $\theta = -19.29$ K (Figure 5b). The negative Weiss constant also manifests the occurrence of the antiferromagnetic interactions within Co^{II} centers. Similar antiferromagnetic couplings within Co^{II} centers have been observed in $Na_5[Co_6(H_2O)_{30}\{Co_9Cl_2(OH)_3(H_2O)_9(\beta\text{-}SiW_8O_{31})_3\}]\cdot37H_2O$[7i] and $K_{12}Li_{16}Co_2[Co_4(H_2O)_{16}P_8W_{48}O_{184}]\cdot60H_2O$.[21]

The magnetic behavior of **2** is shown in Figure 6 as plots of $\chi_M T$ against T and χ_M^{-1} against T. The value of $\chi_M T$ versus the temperature has a constant value of 41.88 emu K mol^{-1} from room temperature to ca. 150 K. This value is close to the expected value (39.38 emu K mol^{-1}) for nine noninteracting $S = {}^5/_2$ Mn^{II} centers considering $g = 2$. Between 150 and ca. 90 K, $\chi_M T$ drops softly, and below 90 K, $\chi_M T$ drops very sharply to reach a value of

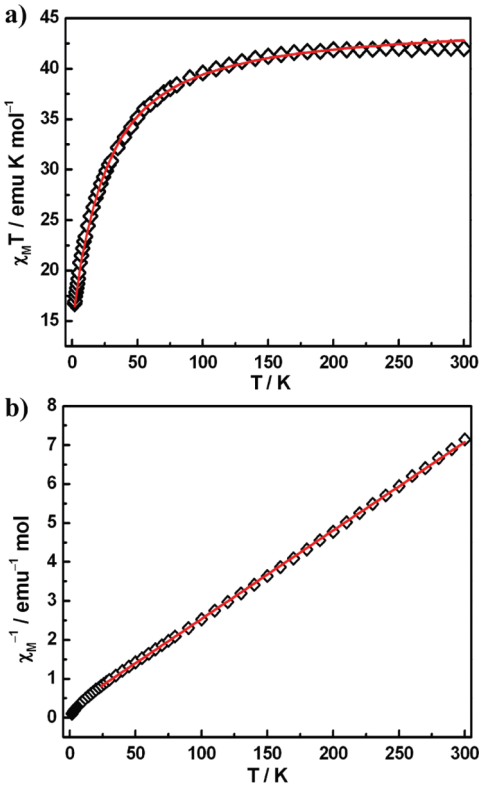

Figure 6. (a) Temperature dependence of the magnetic susceptibility for **2** between 2 and 300 K. The red solid line represents the best fit to experimental data. (b) Temperature evolution of the inverse magnetic susceptibility for **2** between 25 and 300 K. The red solid line was generated from the best fit by the Curie−Weiss expression.

16.73 emu K mol^{-1} at 2 K (Figure 6a). This behavior is indicative of antiferromagnetic exchange interactions among Mn^{II} ions. The magnetic susceptibility data between 25 and 300 K are well described by the Curie−Weiss expression with Curie constant C = 44.04 emu K mol^{-1} and Weiss constant θ = −11.82 K (Figure 6b), which further supports the presence of antiferromagnetic interactions among Mn^{II} centers.

In order to quantitatively analyze magnetic coupling interactions within Mn^{II} centers, we examine the structural parameters of **2**. As seen from the structure of **2** (Figure 3a), three Mn^{II} ions (Mn1, Mn1A, Mn5) are far from each other (Mn1···Mn5: 6.5 Å, Mn1A···Mn5: 6.5 Å, Mn1···Mn1A: 13.0 Å), and they are also far (ca. 6.5 Å and 10.0 Å) from two tri-Mn^{II} clusters sandwiched by [B-β-SiW$_9$O$_{34}$]$^{10-}$ and [B-β-SiW$_8$O$_{31}$]$^{10-}$ fragments, suggesting that, magnetically, they act as independent paramagnetic ions. Therefore, the total magnetic susceptibility is taken as a sum of two tri-Mn^{II} clusters and three uncoupled paramagnetic Mn^{II} ions. Because

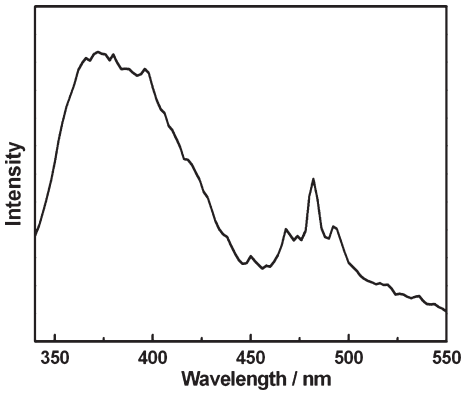

Figure 7. Emission spectrum of **3** in the solid state at room temperature.

the magnetic exchange interactions within the tri-Mn^{II} clusters are mediated through the oxo-bridges, it is important to examine bond distances and angles. Since **2a** is centric, two tri-Mn^{II} clusters incorporated into asymmetric sandwich-type moieties are structurally equivalent. In each tri-Mn^{II} cluster, the structural parameters from single-crystal structural analysis are as follows: Mn2···Mn3, 3.17 Å; Mn3···Mn4, 3.18 Å; Mn4···Mn2, 3.21 Å; ∠Mn2−O64−Mn3, 95.7°; ∠Mn2−O65−Mn3, 92.4°; ∠Mn3−O15−Mn4, 92.0°; ∠Mn3−O65−Mn4, 91.4°; ∠Mn4−O13−Mn2, 94.5°; and ∠Mn4−O65−Mn2, 93.9°. As shown above, based on the fact that the small differences of the Mn···Mn distances and Mn−O−Mn bond angles can be neglected, as a result, we suppose that the tri-Mn^{II} triangle is equilateral and magnetic exchange interactions between Mn2···Mn3, Mn3···Mn4, Mn4···Mn2, Mn2A···Mn3A, Mn3A···Mn4A, and Mn4A···Mn2A are equal. On this assumption, there exists only one exchange constant (J) within two tri-Mn^{II} clusters. Thus, the isotropic spin Hamiltonian for either of two tri-Mn^{II} clusters is described as follows:

$$H = -2J(S_1S_2 + S_2S_3 + S_3S_1) \quad (1)$$

Substitution of the eigenvalues of eq 1 into the standard Van Vleck equation yields the expression of molar magnetic susceptibility (χ_{trimer}) for one tri-Mn^{II} cluster, as shown in eq 2:[20b]

$$\chi_{trimer} = \frac{Ng^2\beta^2}{3kT} \cdot \frac{\{\sum S_n^T(S_n^T+1)(2S_n^T+1)\exp[-E_n kT]\}}{\{\sum(2S_n^T+1)\exp[-E_n/kT]\}} \quad (2)$$

Here, N is Avogadro's number, k is the Boltzmann constant, T is the temperature in Kelvin, and E_n is the spin exchange energy associated with a spin state S_n^T. The final expression of the molar susceptibility for one tri-Mn^{II} cluster is displayed in eq 3:

$$\begin{aligned}\chi_{trimer} &= \frac{Ng^2\beta^2}{3kT} \times \frac{3+60e^{3J/kT}+315e^{8J/kT}+630e^{15J/kT}+990e^{24J/kT}+1287e^{35J/kT}+1365e^{48J/kT}+1020e^{63J/kT}}{4+16e^{3J/kT}+36e^{8J/kT}+40e^{15J/kT}+40e^{24J/kT}+36e^{35J/kT}+28e^{48J/kT}+16e^{63J/kT}} \\ &= \frac{Ng^2\beta^2}{4kT} \times \frac{1+20e^{3J/kT}+105e^{8J/kT}+210e^{15J/kT}+330e^{24J/kT}+429e^{35J/kT}+455e^{48J/kT}+340e^{63J/kT}}{1+4e^{3J/kT}+9e^{8J/kT}+10e^{15J/kT}+10e^{24J/kT}+9e^{35J/kT}+7e^{48J/kT}+4e^{63J/kT}}\end{aligned} \quad (3)$$

dx.doi.org/10.1021/cg200077r |Cryst. Growth Des. 2011, 11, 1913–1923

The experimental $\chi_M T$ data for **2** have been fitted to the magnetic susceptibility expression given in eq 4,

$$\chi_M T = 2\chi_{trimer} T + 3\frac{Ng^2\beta^2 S(S+1)}{3k} \quad (4)$$

where the first term refers to the sum of the products of the susceptibility and temperature of two tri-Mn^{II} clusters and the second one represents three paramagnetic Mn^{II} contributions.

A very satisfying description of the magnetic data over the whole temperature range (red solid line in Figure 6a) has been obtained from the following set of parameters: $J = -1.16$ cm^{-1} and $g = 2.13$. The negative J value confirms the antiferromagnetic coupling interactions among the Mn^{II} centers. The exchange constant J is antiferromagnetic and very close to those previously reported for $[Mn_4(H_2O)_2(PW_9O_{34})]^{10-}$,[22a] $[Mn_4(H_2O)_2(P_2W_{15}O_{56})_2]^{16-}$,[22b] $[\{SiMn_2W_9O_{34}(H_2O)\}_2]^{7e-}$,[12] and $[Mn_4(H_2O)_2(GeW_9O_{34})_2]^{12-}$.[22c] The weak value of the exchange parameter is comparable to those reported in other Mn^{II} clusters with near 90° superexchange paths.[22d]

Photoluminescence. d^{10} polynuclear Cd(II) complexes generally exhibit rich photophysical properties and recently have attracted some attention on both a theoretical and a spectroscopic level.[23] As a result, the solid-state photoluminescence of **3** has been investigated at room temperature (Figure 7). Upon excitation at 320 nm, **3** displays two obvious fluorescence emission bands at 385 and 482 nm, respectively. Evidently, the emission band at 482 nm accompanies two shoulders at 468 and 493 nm. To understand the nature of the two emission bands, the solid-state photoluminescence properties of $3CdSO_4 \cdot 8H_2O$ and $Na_{10}[\alpha\text{-}SiW_9O_{34}] \cdot 18H_2O$ have also been analyzed. $3CdSO_4 \cdot 8H_2O$ displays a broad fluorescence emission band at 330 nm under 240 nm excitation (Figure S7, Supporting Information). $Na_{10}[\alpha\text{-}SiW_9O_{34}] \cdot 18H_2O$ exhibits an intense fluorescence emission band at 480 nm with two shoulders at 466 and 496 nm upon excitation at 320 nm (Figure S8, Supporting Information). On one hand, in comparison with the emission spectrum of **3** with that of $3CdSO_4 \cdot 8H_2O$, the emission band at 385 nm may be ascribed to the O → Cd ligand-to-metal charge transfer (LMCT) transitions, which is also coincident with the reported cadmium(II)-containing compounds.[23c,d] As we know, the Cd^{II} metal dication contains a d^{10} closed shell electronic configuration; thus, d−d transitions are not expected. LMCT transitions usually involve transitions from p(ligand) to d(metal) orbitals and the low-lying s or p empty orbitals of the central metal ion.[23b] Compared with $3CdSO_4 \cdot 8H_2O$, a bathochromic shift of the emission band occurs in **3**, which is probably due to the coordination of Cd^{II} ions to the $[B\text{-}\alpha\text{-}SiW_9O_{34}]^{10-}$ fragments because the emission behavior is closely associated with the coordination environments of the metal ions and the ligands.[24] On the other hand, comparing the photoluminescence spectrum of **3** with that of $Na_{10}[\alpha\text{-}SiW_9O_{34}] \cdot 18H_2O$, the emission band at 482 nm with two shoulders at 468 and 493 nm is induced by $^3T_{1u} \rightarrow {}^1A_{1g}$ transitions derived the O → W LMCT transitions of silicotungstates,[25] which agrees with the fact that **3** contains $[B\text{-}\alpha\text{-}SiW_9O_{34}]^{10-}$ fragments. When several energy levels exist within the O → M (M = Nb, Mo, W) LMCT bands in the POM lattices, energy transfer from the O → M LMCT excited states to these levels may be possible. This process has been observed in the sensitized luminescence Eu^{III}, Mn^{IV}, and Cr^{III} POMs as a result of intramolecular energy transfer.[26] Photoexcitation of the O → M LMCT bands leads to a broad emission due to the $^3T_{1u} \rightarrow {}^1A_{1g}$ transitions, which originate from the O → M LMCT triplet states.[26] All of these suggest that **3** may be suitable as excellent candidates of fluorescent materials.

CONCLUSIONS

By increasing the molar ratios of TM cations/dilacunary Keggin precursors being higher than 5, three novel TMSPs based on Keggin fragments have been prepared and characterized by ICP analyses, IR spectra, UV spectra, and single-crystal X-ray diffraction. The skeleton of **1** is a new trimer consisting of three mono-Co^{II} substituted Keggin fragments $[\alpha\text{-}GeW_{11}CoO_{38}]^{4-}$ linked by six W−O−Co/W bridges and a capping $[Co(H_2O)_3]^{2+}$ bridge. **2** is the first one-dimensional silicotungstate containing asymmetric sandwich-type moieties constructed from $[B\text{-}\beta\text{-}SiW_9O_{34}]^{10-}$ and $[B\text{-}\beta\text{-}SiW_8O_{31}]^{10-}$ fragments. **3** represents the first two-dimensional (3,6)-topological network with a Schläfli symbol of $3^64^65^3$ built by sandwich-type Keggin units in POM chemistry. Magnetic measurements indicate the antiferromagnetic exchange interactions within Co^{II} ions in **1** and within Mn^{II} ions in **2**. Furthermore, the room-temperature solid-state photoluminescence of **3** displays two emission bands, which are derived from O → Cd ligand-to-metal charge transfer (LMCT) transitions and O → W LMCT transitions, respectively. In future work, the reactions of TM ions with dilacunary Keggin precursors will be sufficiently exploited using the principle of chemical equilibrium. We will also explore the reactions of lanthanide ions with dilacunary Keggin precursors.

ASSOCIATED CONTENT

Supporting Information. X-ray crystallographic files for **1**−**3** in CIF format and additional spectroscopic figures. This material is available free of charge via the Internet at http://pubs.acs.org.

AUTHOR INFORMATION

Corresponding Author

*E-mail: zhaojunwei@henu.edu.cn, jyniu@henu.edu.cn. Fax: (+86) 378 3886876.

ACKNOWLEDGMENT

This work was supported by the Natural Science Foundation of China (21071042, 21071043), the China Postdoctoral Science Foundation funded project (20100470996), the Natural Science Foundation of Henan Province (No. 092300410119, 102300410093), the Natural Science Foundation of Henan University (No. 2008YBZR010), the Postdoctoral Science Foundation of Henan University (No. BH2010003), the Foundation of the Education Department of Henan Province (No. 2009A150003, 2010B150006), and the Students Innovative Pilot Plan of Henan University (No. 09NB005).

REFERENCES

(1) (a) *Polyoxometalates: from Platonic Solids to Anti-Retroviral Activity*; Pope, M. T., Müller, A., Eds.; Kluwer: Dordrecht, The Netherlands, 1994. (b) Nishiyama, Y.; Nakagawa, Y.; Mizuno, N. *Angew. Chem., Int. Ed.* **2001**, *40*, 3639.(c) *Polyoxometalate Chemistry: From Topology via Self-Assembly to Applications*; Pope, M. T., Müller, A., Eds.; Kluwer: Dordrecht, 2001. (d) Contant, R.; Hervé, G. *Rev. Inorg. Chem.* **2002**, *22*, 63. (e) Kortz, U.; Hussain, F.; Reicke, M. *Angew. Chem., Int. Ed.* **2005**,

44, 3773. (f) Zhao, J. W.; Jia, H. P.; Zhang, J.; Zheng, S. T.; Yang, G. Y. *Chem.—Eur. J.* **2007**, *13*, 10030. (g) Zhang, Z.-M.; Yao, S.; Li, Y.-G.; Wang, Y.-H.; Qi, Y.-F.; Wang, E.-B. *Chem. Commun.* **2008**, 1650. (h) Duan, C. Y.; Wei, M. L.; Guo, D.; He, C.; Meng, Q. J. *J. Am. Chem. Soc.* **2010**, *132*, 3321. (i) Guo, D. J.; Fu, S. J.; Tan, W.; Dai, Z. D. *J. Mater. Chem.* **2010**, *20*, 10159.

(2) (a) Mialane, P.; Dolbecq, A.; Marrot, J.; Rivière, E.; Sécheresse, F. *Angew. Chem., Int. Ed.* **2003**, *42*, 3523. (b) Mal, S. S.; Kortz, U. *Angew. Chem., Int. Ed.* **2005**, *44*, 3777. (c) Godin, B.; Chen, Y.; Vaissermann, J.; Ruhlmann, L.; Verdaguer, M.; Gouzerh, P. *Angew. Chem., Int. Ed.* **2005**, *44*, 3072. (d) Fang, X.; Anderson, T. M.; Hou, Y.; Hill, C. L. *Chem. Commun.* **2005**, 5044. (e) Nellutla, S.; Tol, J. V.; Dalal, N. S.; Bi, L. H.; Kortz, U.; Keita, B.; Nadjo, L.; Khitrov, G. A.; Marshall, A. G. *Inorg. Chem.* **2005**, *44*, 9795. (f) Yamase, T.; Fukaya, K.; Nojiri, H.; Ohshima, Y. *Inorg. Chem.* **2006**, *45*, 7698. (g) Zhang, Z.; Li, Y.; Wang, E.; Wang, X.; Qin, C.; An, H. *Inorg. Chem.* **2006**, *45*, 4313. (h) Pradeep, C. P.; Long, D. L.; Kögerler, P.; Cronin, L. *Chem. Commun.* **2007**, 4254. (i) Zhang, Z.; Qi, Y.; Qin, C.; Li, Y.; Wang, E.; Wang, X.; Su, Z.; Xu, L. *Inorg. Chem.* **2007**, *46*, 8162. (j) Zhao, J. W.; Li, B.; Zheng, S. T.; Yang, G. Y. *Cryst. Growth Des.* **2007**, *7*, 2658. (k) Zhao, J. W.; Wang, C. M.; Zhang, J.; Zheng, S. T.; Yang, G. Y. *Chem.—Eur. J.* **2008**, *14*, 9223. (l) Zhao, J. W.; Zhang, J.; Zheng, S. T.; Yang, G. Y. *Chem. Commun.* **2008**, 570. (m) Nsouli, N. H.; Ismail, A. H.; Helgadottir, I. S.; Dickman, M. H.; Clemente-Juan, J. M.; Kortz, U. *Inorg. Chem.* **2009**, *48*, 5884.

(3) Nsouli, N. H.; Bassil, B. S.; Dickman, M. H.; Kortz, U.; Keita, B.; Nadjo, L. *Inorg. Chem.* **2006**, *45*, 3858.

(4) (a) Bi, L.-H.; Chubarova, E. V.; Nsouli, N. H.; Dickman, M. H.; Kortz, U.; Keita, B.; Nadjo, L. *Inorg. Chem.* **2006**, *45*, 8575. (b) Nsouli, N. H.; Mal, S. S.; Dickman, M. H.; Kortz, U.; Keita, B.; Nadjo, L.; Clemente-Juan, J. M. *Inorg. Chem.* **2007**, *46*, 8763.

(5) Mitchell, S. G.; Khanra, S.; Miras, H. N.; Boyd, T.; Long, D.-L.; Cronin, L. *Chem. Commun.* **2009**, 2712.

(6) Tézé, A. *Inorganic Syntheses*; John Wiley & Sons: New York, 1990; Vol. 27, p 88.

(7) (a) Zhang, X.-Y.; O'Connor, C. J.; Jameson, G. B.; Pope, M. T. *Inorg. Chem.* **1996**, *35*, 30. (b) Wassermann, K.; Lunk, H.-J.; Palm, R.; Fuchs, J.; Steinfeldt, N.; Stösser, R.; Pope, M. T. *Inorg. Chem.* **1996**, *35*, 3273. (c) Xin, F.; Pope, M. T. *Inorg. Chem.* **1996**, *35*, 5693. (d) Kortz, U.; Jeannin, Y. P.; Tézé, A.; Hervé, G.; Isber, S. *Inorg. Chem.* **1999**, *38*, 3670. (e) Kortz, U.; Isber, S.; Dickman, M. H.; Ravot, D. *Inorg. Chem.* **2000**, *39*, 2915. (f) Kortz, U.; Matta, S. *Inorg. Chem.* **2001**, *40*, 815. (g) Hussain, F.; Bassil, B. S.; Bi, L.-H.; Reicke, M.; Kortz, U. *Angew. Chem., Int. Ed.* **2004**, *43*, 3485. (h) Kamata, K.; Yonehara, K.; Sumida, Y.; Yamaguchi, K.; Hikichi, S.; Mizuno, N. *Science* **2003**, *300*, 964. (i) Bassil, B. S.; Nellutla, S.; Kortz, U.; Stowe, A. C.; van Tol, J.; Dalal, N. S.; Keita, B.; Nadjo, L. *Inorg. Chem.* **2005**, *44*, 2659. (j) Bassil, B. S.; Kortz, U.; Tigan, A. S.; Clemente-Juan, J. M.; Keita, B.; de Oliveira, P.; Nadjo, L. *Inorg. Chem.* **2005**, *44*, 9360. (k) Bassil, B. S.; Dickman, M. H.; Kortz., U. *Inorg. Chem.* **2006**, *45*, 2394. (l) Botar, B.; Geletii, Y. V.; Kögerler, P.; Musaev, D. G.; Morokuma, K.; Weinstock, I. A.; Hill, C. L. *J. Am. Chem. Soc.* **2006**, *128*, 11268. (m) Botar, B.; Kö1gerler, P.; Hill, C. L. *Inorg. Chem.* **2007**, *46*, 5398. (n) Mialane, P.; Duboc, C.; Marrot, J.; Rivière, E.; Dolbecq, A.; Sécheresse, F. *Chem.—Eur. J.* **2006**, *12*, 1950. (o) Lisnard, L.; Mialane, P.; Dolbecq, A.; Marrot, J.; Clemente-Juan, J. M.; Coronado, E.; Keita, B.; de Oliveira, P.; Nadjo, L.; Sécheresse, F. *Chem.—Eur. J.* **2007**, *13*, 3525. (p) Zhao, J. W.; Zheng, S. T.; Yang, G. Y. *J. Solid State Chem.* **2008**, *181*, 2205.

(8) (a) Sheldrick, G. M. *SHELXS 97, Program for Crystal Structure Solution*; University of Göttingen: Göttingen, Germany, 1997. (b) Sheldrick, G. M. *SHELXL 97, Program for Crystal Structure Refinement*; University of Göttingen, Germany, 1997.

(9) (a) Reinoso, S.; Vitoria, P.; Felices, L. S.; Lezama, L.; Gutiérrez-Zorrilla, J. M. *Chem.—Eur. J.* **2005**, *11*, 1538. (b) Lu, Y.; Xu, Y.; Wang, E. B.; Lü, J.; Hu, C. W.; Xu, L. *Cryst. Growth Des.* **2005**, *5*, 257.

(10) Zhang, Z.; Yao, S.; Wang, E.; Qin, C.; Qi, Y.; Li, Y.; Clérac, R. *J. Solid State Chem.* **2008**, *181*, 715.

(11) Mitchell, S. G.; Ritchie, C.; Long, D.-L.; Cronin, L. *Dalton Trans.* **2008**, 1415.

(12) Weakley, T. J. R.; Evans, H. T., Jr.; Showell, J. S.; Tourné, G. F.; Tourné, C. M. *J. Chem. Soc., Chem. Commun.* **1973**, 139.

(13) Zhao, J. W.; Li, J. L.; Ma, P. T.; Wang, J. P.; Niu, J. Y. *Inorg. Chem. Commun.* **2009**, *12*, 450.

(14) Dolomanov, O. V.; Blake, A. J.; Champness, N. R.; SchrNder, M. *J. Appl. Crystallogr.* **2003**, *36*, 1283.

(15) Haraguchi, N.; Okaue, Y.; Isobe, T.; Matsuda, Y. *Inorg. Chem.* **1994**, *33*, 1015.

(16) Niu, J. Y.; Wang, K. H.; Chen, H. N.; Zhao, J. W.; Ma, P. T.; Wang, J. P.; Li, M. X.; Bai, Y.; Bang, D. B. *Cryst. Growth Des.* **2009**, *9*, 4362.

(17) Hervé, G.; Tézé, A. *Inorg. Chem.* **1977**, *16*, 2115.

(18) (a) Wang, J. P.; Duan, X. Y.; Du, X. D.; Niu, J. Y. *Cryst. Growth Des.* **2006**, *6*, 2266. (b) Wang, J. P.; Zhao, J. W.; Duan, X. Y.; Niu, J. Y. *Cryst. Growth Des.* **2006**, *6*, 507.

(19) (a) Ritorto, M. D.; Anderson, T. M.; Neiwert, W. A.; Hill, C. L. *Inorg. Chem.* **2004**, *43*, 44. (b) Bösing, M.; Nöh, A.; Loose, I.; Krebs, B. *J. Am. Chem. Soc.* **1998**, *120*, 7252.

(20) (a) Carlin, R. L. *Magnetochemistry*; Springer-Verlag: New York, 1983. (b) Kahn, O. *Molecular Magnetism*; VCH: New York, 1993.

(21) Bassil, B. S.; Ibrahim, M.; Mal, S. S.; Suchopar, A.; Biboum, R. N.; Keita, B.; Nadjo, L.; Nellutla, S.; van Tol, J.; Dalal, N. S.; Kortz, U. *Inorg. Chem.* **2010**, *49*, 4949.

(22) (a) Gómez-García, C. J.; Coronado, E.; Gómez-Romero, P.; Casañ-Pastor, N. *Inorg. Chem.* **1993**, *32*, 3378. (b) Gómez-García, C. J.; Borrás-Almenar, J. J.; Coronado, E.; Ouahab, L. *Inorg. Chem.* **1994**, *33*, 4016. (c) Kortz, U.; Nellutla, S.; Stowe, A. C.; Dalal, N. S.; Rauwald, U.; Danquah, W.; Ravot, D. *Inorg. Chem.* **2004**, *43*, 2308. (d) Smit, J. J.; Nap, G. M.; de Jongh, L. J.; van Ooijen, J. A. C.; Reedijk, J. *Physica* **1979**, *97B*, 365.

(23) (a) Zheng, S. L.; Chen, X. M. *Aust. J. Chem.* **2004**, *57*, 703. (b) Barbieri, A.; Accorsi, G.; Armaroli, N. *Chem. Commun.* **2008**, 2185. (c) Du, Z. Y.; Li, X. L.; Liu, Q. Y.; Mao, J. G. *Cryst. Growth Des.* **2007**, *7*, 1501. (d) Su, Y.; Zang, S.; Li, Y.; Zhu, H.; Meng, Q. 2007, *7*, 1277.

(24) (a) Wang, X.-L.; Qin, C.; Li, Y.-G.; Hao, N.; Hu, C.-W.; Xu, L. *Inorg. Chem.* **2004**, *43*, 1850. (b) Dai, J.-C.; Wu, X.-T.; Fu, Z.-Y.; Cui, C.-P.; Wu, S.-M.; Du, W.-X.; Wu, L.-M.; Zhang, H.-H.; Sun, Q. *Inorg. Chem.* **2002**, *41*, 1391.

(25) Ito, T.; Yashiro, H.; Yamase, T. *Langmuir* **2006**, *22*, 2806.

(26) Yamase, T. *Chem. Rev.* **1998**, *98*, 307.